An Analytical Equivalent Circuit Representation for Waveguide-Mounted Gunn Oscillators

C. P. JETHWA, STUDENT MEMBER, IEEE, AND ROBERT L. GUNSHOR, MEMBER, IEEE

Abstract—A lumped equivalent circuit is used to represent the impedance presented to the device terminals for a waveguide-mounted Gunn oscillator. Analytic expressions are used for all the lumped elements. This circuit model is used to predict tuning curves which are compared to experimental tuning curves obtained for iris coupling, for full- and reduced-height waveguides, and for various post diameters. Iris-controlled nontunable modes are reported and explained by the model. The real part of the load impedance presented at the device terminals is found to agree with Copeland's prediction for optimum loading. Experimentally observed mode switching is explained with reference to variations in device parameters.

I. Introduction

IN ORDER TO understand the interactions between a high-frequency device, such as a tunnel diode, Gunn diode, or avalanche diode, and the microwave structure in which the device is mounted, it is essential to know the radiation impedance at the device terminals presented by the microwave circuit.

The first attempt at deriving an analytical expression for this impedance was reported by Yamashita and Baird [1]. They obtained a dyadic Green's function to evaluate the impedance at the device terminals for microwave structures in which the ratio of height to width could be assumed small compared to a full-height waveguide.

Hanson and Rowe [2] extended Yamashita and Baird's [1] analysis to microwave structures of standard waveguide dimensions. Both of these apply for a centered post and where the device is mounted at a broad wall of the waveguide.

Eisenhart and Khan [3] carried out a theoretical analysis, based on a dyadic Green's function, to characterize a more general waveguide mount configuration in which the post supporting the device can be located anywhere along the broad dimension of the waveguide and the device could be positioned anywhere along the post.

In order to reduce the complex mathematics associated with the dyadic Green's function approach to a manageable form, all three of these analyses neglected the phase variation of the field across the post (thin post assumption)[1] in the direction of propagation of the dominant waveguide mode.

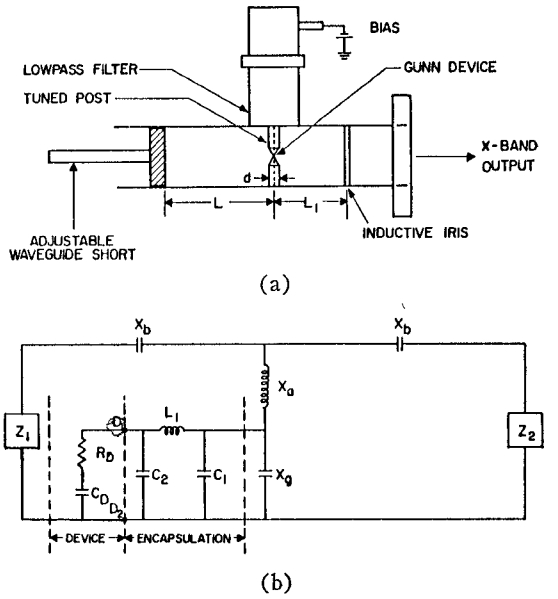

Fig. 1. (a) Waveguide-mounted Gunn oscillator configuration. Low-pass filter cutoff is at 6 GHz. Waveguide is RG 52/u and iris opening is 0.65 cm. (b) Equivalent circuit for the waveguide-mounted Gunn oscillator. For the Mullard devices $C_D=0.2$ pF, $R_D=-4\ \Omega$, $L_1=0.65$ nH, $C_1=0.10$ pF, $C_2=0.12$ pF [6]. For the Watkins–Johnson devices a parallel circuit device representation is used with $C_{Dp}=0.24$ pF, $R_{Dp}=-100\ \Omega$, $L_1=0.42$ nH, $C_1=0.18$ pF, $C_2=0$ [7].

Tsai *et al.* [4] have used experimentally determined components for an equivalent circuit to represent the waveguide mount.

Because of the unavailability of a complete mathematical solution for treating the finite-diameter post,[2] an alternate approach is presented [6]. Our experimental configuration for the X-band CW Gunn-effect oscillator is shown in Fig. 1(a) and the equivalent circuit shown in Fig. 1(b). Two types of X-band CW Gunn devices were used. One type was made by Mullard; the other was donated by Watkins–Johnson. Several of each type were used in obtaining the experimental re-

Manuscript received August 9, 1971; revised February 9, 1972. This work was supported in part by the Advanced Research Projects Agency under the Purdue University program and in part by the National Science Foundation under Grant GK-11958.

The authors are with the School of Electrical Engineering, Purdue University, Lafayette, Ind. 47907.

[1] Throughout the paper, a thin post represents an obstacle with zero thickness in the direction of propagation of the dominant waveguide mode.

[2] Bradshaw has recently extended Lewin's theory to predict the scattering for a finite-diameter tuned post [5].

sults reported here. The Watkins–Johnson diodes were used mainly for comparison with the Mullard devices which, unless otherwise specified, were used to obtain most of the experimental data.

II. Theoretical Circuit Model

The lumped equivalent circuit representation of the waveguide-mounted Gunn oscillator is shown in Fig. 1(b). The circuit elements L_1, C_1, and C_2 constitute a π-equivalent circuit representation as published by Mullard [7] for the encapsulation of their CXY11/A series of X-band Gunn devices. In this figure, as suggested by Mullard [7], the Gunn device is represented by a series circuit consisting of a negative resistance R_D and an effective device capacitance C_D. One could equivalently represent the device by a circuit with a negative conductance shunted by an appropriate device capacitance as discussed in Section III. The device parameters suggested by Watkins–Johnson [8] are appropriate to the shunt representation.[3]

The device is supported in the waveguide by means of a metallic post of diameter d. Such a post with the device removed is called a tuned post and is represented by a T network composed of the series reactances X_b and a shunt reactance consisting of the series combination of X_a and X_g. The phase variation of the field across the post in the direction of propagation, caused by the finite diameter of the post, is accounted for by the series capacitive reactances X_b. The shunt inductive reactance element X_a represents magnetic energy storage associated with the evanescent TE_{m0} modes ($m>1$).

In our analysis of the diode mount, X_a and X_b are the elements resulting from the constant current component of the total current and are described by Marcuvitz [9] for a finite-diameter post which completely spans the waveguide. The addition of the gap in this post for mounting the device causes a deviation from constant current, producing a capacitive energy storage represented by X_g. The voltage-power absolute impedance definition for the waveguide is used. Thus the TE_{10} mode waveguide impedance is

$$Z_0 = 240\pi(b/a)(\lambda_g/\lambda).$$

Eisenhart and Khan [3] have used a dyadic Green's function technique to derive impedance expressions for a tuned thin post. Employing an equivalence between a thin post and the corresponding circular post [3], [10], Eisenhart and Khan's resulting expression for the gap reactance X_g is used in our model.

The combination of the Marcuvitz [9] and the Eisenhart and Khan [3] theories applies for the post located anywhere along the broad dimension of the waveguide and the device positioned anywhere along the post, and includes the inherent frequency dependence of all elements.

[3] A subscript p will be used in this paper to denote circuit elements used in a parallel configuration.

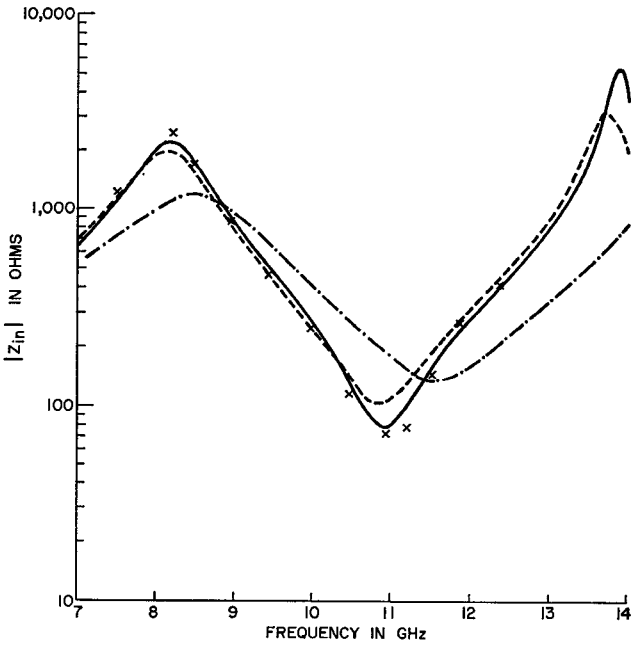

Fig. 2. Impedance magnitude of the tuned post as a waveguide obstacle referred to the flange plane. ——— Theory with X_b and X_g included. ------ Theory with $X_b=0$ and X_g included. —·—· Theory with gap represented as parallel plate capacitor. × Experimental results.

The impedance due to the variable waveguide short, referred to the plane of the device, is represented by Z_1. Similarly, the load impedance due to the parallel combination of the TE_{10} mode waveguide impedance Z_0, and the inductive reactance of the iris [9], referred to the plane of the device, is represented by Z_2.

Tsai *et al.* [4] have recently proposed a similar equivalent circuit, determining the parameters of the tuned post experimentally, and treating them as frequency independent elements. Calculations show that these parameters are frequency dependent, with values for the post inductance varying 30 percent over the 8–12-GHz range, while the series capacitances ($1/\omega X_b$) have a 100-percent variation for this frequency range.

A simple test of the validity of the model consists of measurements using the mounting post as a waveguide obstacle. The justification for such measurements has been expressed by Lewin [11], who says: "A coaxial cable . . . feeds into a waveguide . . . . Alternatively, the waveguide may be considered as feeding via the probe into the cable. It does not matter which way the problem is tackled, and if the target of specifying an equivalent circuit with determinate parameters is achieved, the configuration may be used any way round that may be of use." Thus the device is removed, the tuning short is replaced by a matched termination, and impedance measurements are made. The impedance measurements are referred to the waveguide output flange, and compared to the calculated impedance referred to the same plane in Fig. 2. In Fig. 2 a theoretical

impedance curve obtained by neglecting the phase variation of the field along the post diameter ($X_b=0$) is shown. It is seen that, for a typical post diameter, theory and experiment agree more closely when X_b is not neglected. Also shown is a theoretical curve for the finite post theory considering the gap as a "parallel-plate capacitor" with fringing neglected; this is not at all in agreement with the experiment. This implies that the gap is properly accounted for by using the gap reactance expression derived by Eisenhart and Khan [3].

It is expected that when the device is mounted, the conduction current through the device should improve the assumption of constant current along the post axis, which was the basis for our application of the Marcuvitz theory [9]. It is worth noting that many calculations have shown that the actual significance of the gap reactance is considerably reduced as a result of the shunting effect of the device and encapsulation.

III. Circuit-Controlled Oscillations

The criteria for circuit-controlled steady-state oscillations are well known. These are

$$R_D(\omega) + R_L(\omega) = 0 \tag{1}$$

$$X_D(\omega) + X_L(\omega) = 0. \tag{2}$$

Alternatively, if admittances are used, these are

$$G_{Dp}(\omega) + G_{Lp}(\omega) = 0 \tag{3}$$

$$B_{Dp}(\omega) + B_{Lp}(\omega) = 0 \tag{4}$$

where $R_L(\omega)$ and $X_L(\omega)$ are real and imaginary parts of the load impedance at the device terminals and $R_D(\omega)$ and $X_D(\omega)$ are, respectively, the real and imaginary parts of the device impedance. Similarly, $G_{Lp}(\omega)$ and $B_{Lp}(\omega)$ are the real and imaginary parts of the load admittance at the device terminals and $G_{Dp}(\omega)$ and $B_{Dp}(\omega)$ are, respectively, the real and imaginary parts of the device admittance. $R_D(\omega)$ and $G_{Dp}(\omega)$ are negative quantities. In addition to these requirements for steady-state oscillations, the stability of such circuit-controlled oscillations is governed by the requirement that

$$\frac{\partial X(\omega)}{\partial \omega} > 0 \tag{5}$$

or equivalently [12],

$$\frac{\partial B(\omega)}{\partial \omega} > 0 \tag{6}$$

where $X(\omega)$ is the total reactance $X_L(\omega)+X_D(\omega)$, and B is the total admittance $B_{Lp}(\omega)+B_{Dp}(\omega)$. It can be shown that Kurokawa's [13], [14] more recent work provides the same criteria. It should be noted, however, that these criteria for stability are derived under the assumption that the negative resistance or conductance of the device is frequency independent [12]–[14]. This is, of course, not the case for Gunn devices, although these criteria are generally used to explain the stability of Gunn oscillators.

IV. Tuning Characteristics

First we consider the tuning characteristics of the oscillator without a coupling iris, where the waveguide output is directly terminated with a matched load. The application of the zero total reactance requirement, as given in (2), results in a transcendental equation which is solved numerically to obtain all theoretical tuning curves. The oscillation frequencies are obtained as intersections between $B_{Lp}(\omega)$ and $-B_{Dp}(\omega)$. There are always two such frequencies per cavity mode for a given short position; one satisfies (6), the other does not [4].

The experimental tuning curves are obtained by varying the distance L between the waveguide sliding short and the device plane, with the direction of motion of the short both away from and towards the device plane. Throughout these investigations the bias voltage is held at a constant value of 6.5 V.

Shown in Fig. 3 are theoretical and experimental tuning curves [4], [6], [15]–[17] for two different post diameters, where the device is mounted in the center of the post. Good agreement between theory and experiment is observed. It is seen that both theoretical and experimental tuning curves essentially follow the $n\lambda_g/2$ cavity modes. (As a result, we will identify particular theoretical and experimental tuning curves by the cavity mode closest to them. Thus the $\lambda_g/2$ tuning curve is the tuning curve that is close to the $\lambda_g/2$ cavity mode.) Hysteresis in the experimental tuning curves is observed and mode switching is indicated by arrows [4], [6], [15]–[18]. (Mode switching is discussed in Section VI of this paper.) The theoretical and experimental tuning curves are found to lie below the waveguide modes for smaller post diameters; this effect has been previously reported [4], [15]–[17]. However, it can be seen that for the larger post diameter the theoretical and experimental tuning curves move to a position above the waveguide modes, an effect that can also be seen in the theoretical tuning curves calculated by Eisenhart and Khan [18]. This shift can be regarded as an increase in line length to provide more inductance at a given frequency as X_b increases with increased post diameter.

It is seen that oscillations are not observed experimentally for short positions of less than 1.4 cm for the smaller post diameter, for which it is also found that (2) is not satisfied.

Shown in Fig. 4 are the tuning characteristics for an iris-coupled oscillator, where the device is at the center of the post, positioned equidistant from the broad wall of the waveguide. The case of an inductive iris has been included for generality as such reactive elements are often introduced for impedance matching, to introduce multiple frequency cavities, etc. It is seen that both the theoretical and experimental curves show the existence of a forbidden frequency band from 12.0 to 12.5 GHz.

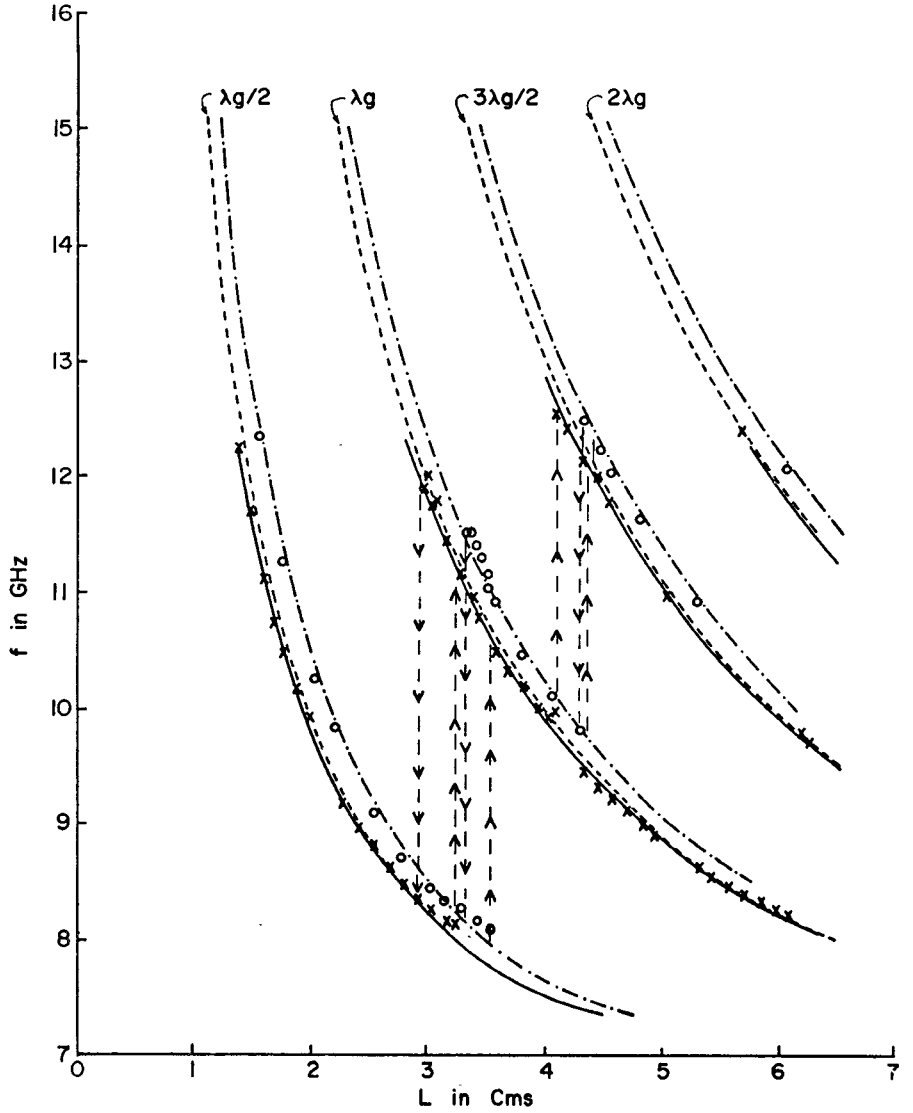

Fig. 3. Tuning curves for full-height waveguide with the iris removed and the device in the center of the post. ——— Theoretical for 0.307-cm post diameter. —·—· Theoretical for 0.52-cm post diameter. ------ $n\lambda_g/2$ cavity modes (n is an integer and λ_g is guide wavelength). × Experimental for 0.307-cm post diameter. o Experimental for 0.52-cm post diameter. (The arrows indicate mode switching.)

Theoretical calculations show that in this frequency range the imaginary part of the load impedance $X_L(\omega)$ is capacitive. Since the imaginary part of the device impedance $X_D(\omega)$ is capacitive for all frequencies, the zero total reactance requirement (2) is not satisfied in this frequency range. It was not possible to obtain any experimental points within the forbidden band, thus providing further confirmation of the accuracy of the theory.

Also seen in Fig. 4 are "iris-controlled" oscillation regions, which are essentially nontunable with respect to short position. The effect of changing the position of the iris relative to the device plane is also shown in this figure. With the iris located 2.9 cm from the device plane, iris-controlled nontunable oscillation frequencies of 8.3 GHz and approximately 12.0 GHz are found. At 8.3 GHz the distance between the device plane and the iris corresponds to an electrical distance of $\lambda_g/2$; at 12.0 GHz this distance represents λ_g. With the distance between the iris and the device plane arbitrarily changed to 4.5 cm, the iris-controlled frequencies become 9.35 and 11.65 GHz. These frequencies are found to correspond to electrical distances of λ_g and $3\lambda_g/2$, respectively. Thus the fixed frequency modes are iris controlled and correspond to cavity resonances formed between the mounted device and a coupling reactance, in this case provided by an inductive iris.

In both Fig. 4 and Fig. 3, two oscillation frequencies are shown for some values of the short position L. The excitation of alternative modes at a given short position depends on the direction of travel of the short. At certain times, simultaneous oscillations at two frequencies are observed for a given value of L.

These tendencies for fixed frequency operation are distinct in nature from the frequency saturation effect reported by Taylor *et al.* [15] and explained by Eisen-

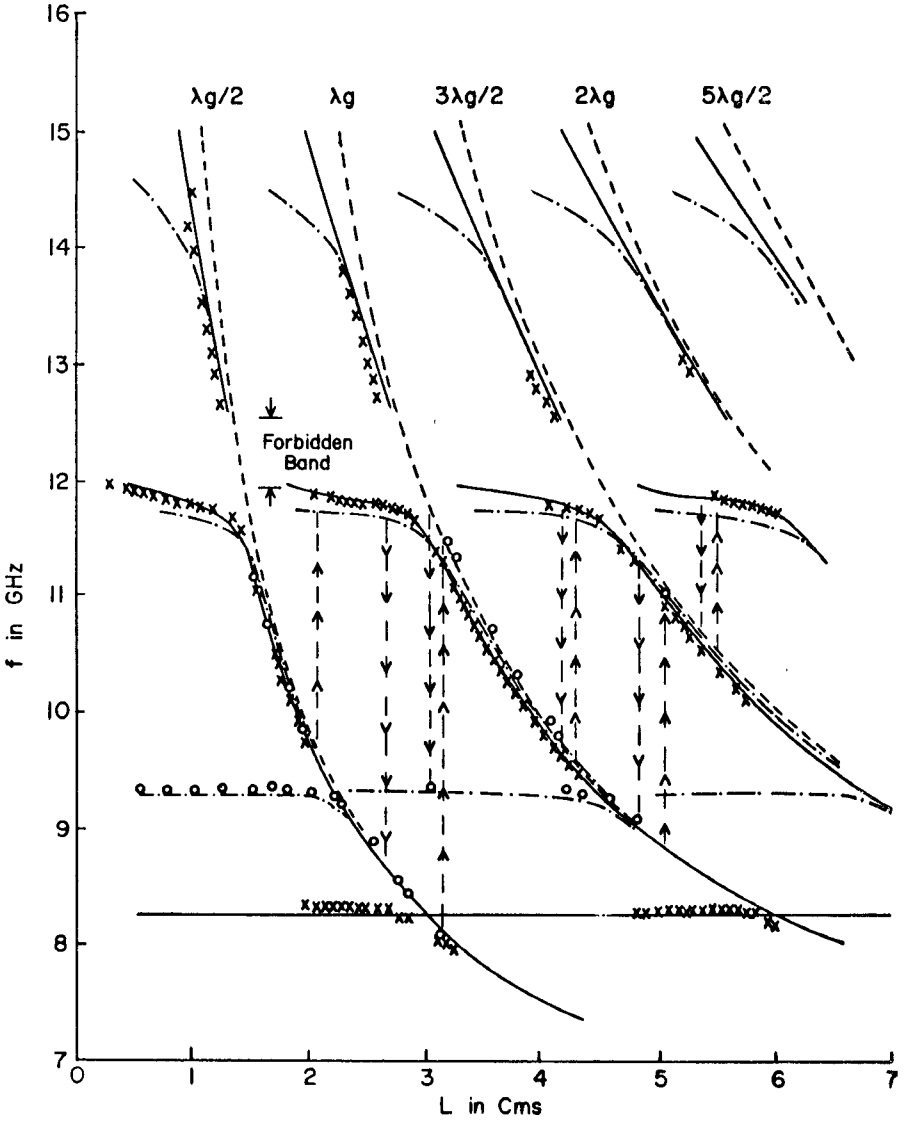

Fig. 4. Tuning curves for a full-height waveguide iris-coupled oscillator with the device in the center of the post. Two iris positions are used with the same post diameter (0.307 cm). ——— Theoretical with iris located 2.9 cm from the device plane. —·—· Theoretical with iris located 4.5 cm from the device plane. ------ $n\lambda_g/2$ cavity modes. × Experimental for iris distance of 2.9 cm. o Experimental for iris distance of 4.5 cm. (Arrows indicate mode switching.) Note the forbidden band and the nontunable regions.

hart and Khan [18]. These iris-controlled regions have serious implications for the tuning of waveguide-mounted oscillators as they tend to capture the oscillation away from the tuning curves following waveguide mode characteristics, thereby interfering with normal tuning. Thus the oscillation energy switches from the short-to-post cavity to the iris-to-post cavity. This type of behavior is to be expected for any lumped discontinuity used for coupling or matching the oscillator.

The diode and encapsulation parameters were varied from the values given in the equation for Fig. 1(b) to observe their effect on the theoretical tuning curves discussed above. It was found that when these parameters were varied by about a factor of 2, the theoretically predicted tuning curves essentially remained unchanged at lower frequencies where they tend to coincide with the $n\lambda_g/2$ waveguide modes. However, at higher frequencies where tuning curves deviate to a greater extent from the waveguide modes, some small variation is observed with a change in diode capacitance. For example, when the encapsulation capacitor values are doubled and the lead inductance is halved, it is found that for frequencies above about 10 GHz, (2) cannot be satisfied and thus oscillation is not predicted.

V. Impedance Presented at Device Terminals

The impedance presented by the microwave circuit to the device terminals is calculated by specifying the position of the short and the corresponding oscillation frequency. These calculations can be performed with both experimental and theoretical tuning curves; for brevity we will discuss only those obtained using experimental tuning curves.

It has been shown by Copeland [19] that for circuit-

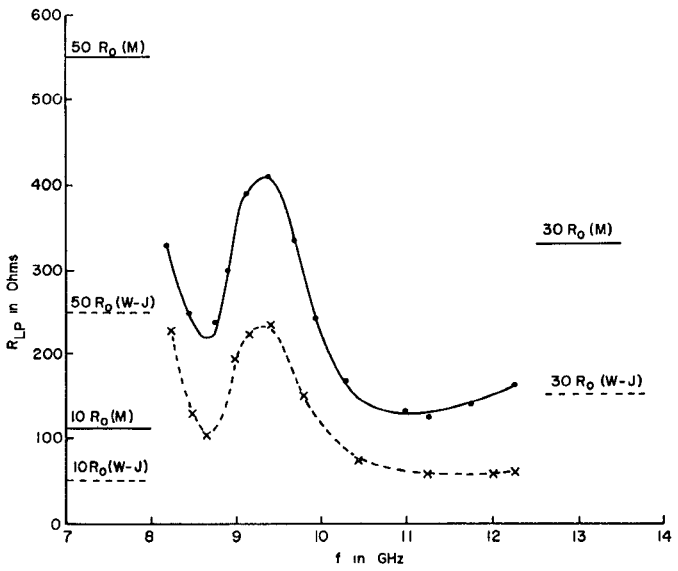

Fig. 5. Real part of the load impedance (R_{Lp}) versus frequency or two different types of devices. ——— $R_0 = 11\ \Omega$ (Mullard). ------ $R_0 = 5\ \Omega$ (Watkins–Johnson).

controlled oscillations the load impedance presented at the device terminals should lie in the range between $10R_0$ and $50R_0$, while for maximum efficiency it should be $30R_0$, where R_0 is the low field resistance of the device.

In Fig. 5, $R_{Lp}(R_{Lp} = 1/G_{Lp})$ versus frequency is plotted for devices with different low field resistance values. One curve is typical for a group supplied by Watkins–Johnson having a low field resistance R_0 of 5 Ω, while the other curve is for Mullard devices for which R_0 is 11 Ω. It is seen that for a given short position, the frequency of oscillation results in values for R_{Lp} which fall within the criteria specified by Copeland [19].

The values obtained differ, depending whether a finite or a thin post theory is used [6]. The degree of difference is found to be a strong function of the reflection coefficient of the sliding short. If the magnitude of reflection coefficient is taken as unity, the thin post theory predicts poles of $R_{Lp}(\omega)$ for certain frequencies on the tuning curves. The thin post theory is especially sensitive to the reflection coefficient; a value of 0.983[4] will considerably improve agreement with finite post theory.

VI. Mode Switching

All experimental tuning curves shown in this paper exhibit mode switching and tuning hysteresis. For simplicity we restrict the discussion of mode switching to oscillators without iris coupling.

In the following discussion we will see the failure of the linear device model to explain or predict mode switching. As previously stated, it is experimentally observed (Fig. 3) that in the regions of mode switching, the tuning curve tends to pull up slightly due to device nonlinearities. We will show that this tends to cause the device susceptance to go towards zero and R_L to rise sharply, although cause and effect cannot really be distinguished.

With reference to Fig. 3 for the smaller post diameters, as tuning is performed by moving the sliding short outward from a position close to the post ($L = 1.35$ cm), the tuning curve essentially follows the $\lambda_g/2$ tuning curve until, at a frequency of 8.18 GHz at $L = 3.20$ cm, a switch to the λ_g tuning curve occurs at a frequency of 11.2 GHz. A similar behavior is observed for the larger diameter post although the mode switch occurs at a lower frequency. When the direction of motion of the short is reversed, say at 4.0 cm, the tuning for the smaller diameter post proceeds along the λ_g curve until a downward mode switch occurs at 11.9 GHz, where the oscillation switches to the $\lambda_g/2$ tuning curve at a frequency of 8.3 GHz. For the larger diameter post, the jump downwards occurs at a lower frequency. Although mode switching is observed to occur between other modes, we restrict our discussion to mode switching between $\lambda_g/2$ and λ_g tuning curves.

An examination of the experimental tuning curves in the region where a mode switch occurs from $\lambda_g/2$ to λ_g reveals that the curves tend to pull upward from the theoretical tuning curves. A similar effect occurs for a switch from λ_g to $\lambda_g/2$, but is less pronounced. This behavior is general, and is observed for both post diameters, and also for reduced-height waveguide tuning curves. This effect is believed to be due to the nonlinear behavior of the device. This conclusion is strongly suggested by the observation of nonsinusoidal device current waveforms (using a magnetic pickup loop and sampling oscilloscope), in the region where the mode jumps occur. For the full-height waveguide, a Fourier analysis of this waveform indicates components at 8.3 and 4.15 GHz. The presence of these components is confirmed by a spectrum analysis of signals in the coaxial bias circuit. We interpret the 4.15-GHz component as subharmonic.

It is interesting to note that for both full- and reduced-height waveguides, the $\lambda_g/2$-to-λ_g mode switch occurs near a value of L corresponding to the intersection of the λ_g mode characteristic with a curve constructed by plotting values of $(3/2)f$ versus L for values of f (frequency) on the $\lambda_g/2$ mode curve. This fact, together with the observed subharmonic, might suggest that a three-frequency process (f, $f/2$, $3f/2$) could be involved in the transfer of energy between modes at the region of the mode switch.

The mode switching can be discussed with reference to (1)–(6). The emphasis in this section is on a description of the conditions that exist during mode switching and a discussion of how these conditions produce mode switching. It is shown that a purely theoretical predic-

[4] This is an experimentally measured value, and is used for all reported calculations.

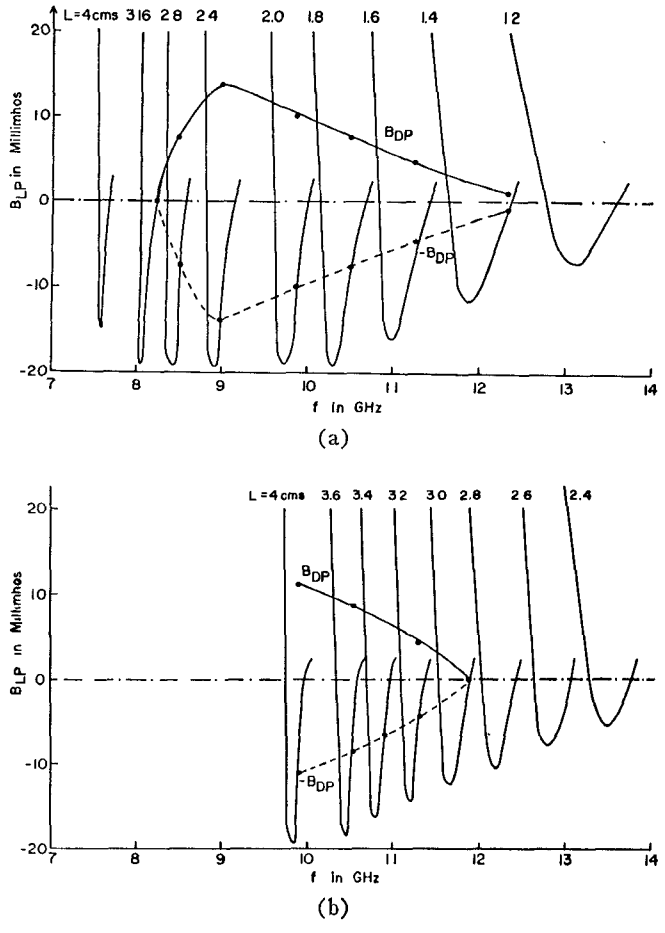

Fig. 6. (a) Set of B_{Lp} versus frequency curves, each for a different short position along the $\lambda_g/2$ tuning curve, for full-height waveguide. The dashed line is $-B_{Dp}$ versus frequency; the opposing solid line shows B_{Dp} versus frequency (0.307-cm post diameter). (b) Same as (a), but drawn for the λ_g tuning curves.

tion of mode switching is not possible since the simple available device models do not include the inherent dynamic nonlinearities of the device. Thus it is not possible to predict *a priori* how the device will respond to, and to what extent it can compensate for, changing circuit conditions.

Fig. 6(a) shows plots of load susceptance B_{Lp} versus frequency corresponding to $\lambda_g/2$ tuning curves for a full-height waveguide oscillator. Also shown in Fig. 6(a) is a plot of device susceptance obtained corresponding to experimental tuning curves. These are drawn between points corresponding to the negative of the load susceptance for a particular short position and a frequency corresponding to experimental tuning curves. In this figure it is seen that as the frequency is decreased, the device susceptance decreases, tending toward zero, while the condition of zero total susceptance (2) continues to be satisfied. However, there is no reason to expect that a Gunn device is capable of presenting a net inductive susceptance. Thus it is seen that (2) cannot be satisfied on the $\lambda_g/2$ tuning curve for frequencies below 8.18 GHz, the frequency at which mode switching is observed for the smaller post (Fig. 3). It is important to note that the stability requirement given by (6) is satisfied because in this region of the curves both the device and load susceptance frequency derivatives are positive. Hence it is concluded that mode switching from the $\lambda_g/2$ to the λ_g tuning curve occurs due to the fact that the oscillation condition given by (2) is not satisfied, rather than that the stability criteria (6) are violated.

When similar curves are drawn for a larger post diameter of 0.52 cm, it is found that (2) is not satisfied at 8.02 GHz, a frequency below the point for the smaller post diameter. This result is seen in Fig. 3 as different mode switch points for the two post diameters.

A similar discussion of mode switching applies to a reduced-height waveguide. It is found that the zero total susceptance condition is not satisfied on the $\lambda_g/2$ tuning curve at a frequency of 9.3 GHz, a higher frequency than in the full-height waveguide case, and at which the mode switching is observed.

Fig. 6(b) is used for a discussion of mode switching from the λ_g down to the $\lambda_g/2$ tuning curve for a full-height waveguide with a post diameter of 0.307 cm. Again it is here seen that as the frequency is increased, the device susceptance decreases, tending toward zero. It is found that at the frequency of 11.9 GHz at which mode switching occurs (Fig. 3), the device susceptance (B_{Dp}) calculated by using this frequency and the corresponding waveguide position ($L=3.00$ cm), approaches zero.

In contrast to the discussion for Fig. 6(a), in Fig. 6(b) the frequency derivative of the device and load susceptances have opposite signs in the mode switching region, and hence the stability condition of (6) must be examined. It is found that the frequency derivative of the device susceptance is not sufficiently negative to overcome the positive derivative of the load susceptance, and thus fails to violate the stability criteria in the region where the mode switching is experimentally observed.

Similar results for mode switching from the λ_g to the $\lambda_g/2$ tuning curve are obtained for reduced-height waveguide. The conclusions are the same as for the full-height waveguide, except that the switch occurs at a higher frequency of 13.65 GHz.

When these calculations are performed for a larger post diameter (0.52 cm) in a full-height waveguide, again similar conclusions are drawn; in this case zero device susceptance occurs at 11.5 GHz.

The real part of the load impedance R_L, presented to the device terminals in the mode switching region is examined, in this case for a Watkins–Johnson device. Tuning curves, X-band power output, and load resistance calculated from the experimental tuning curve, are shown in Fig. 7. In Fig. 7(c), the solid line represents calculations corresponding to the experimental tuning curve close to the $\lambda_g/2$ mode; the dashed curve corresponds to the experimental curve near the λ_g mode. In

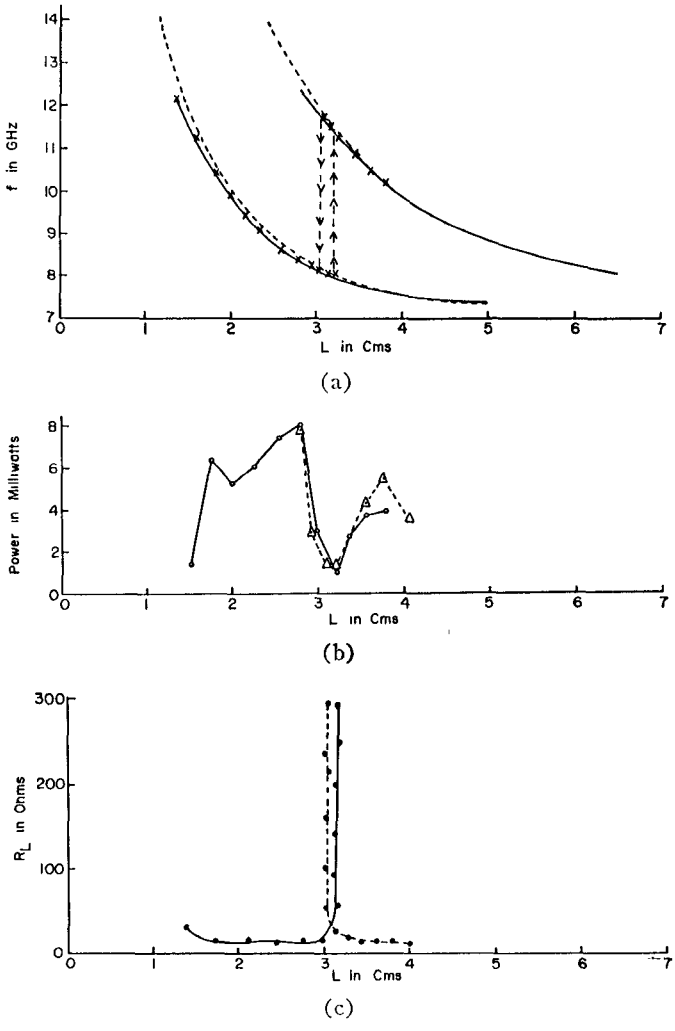

Fig. 7. (a) Experimental and theoretical tuning curves for Watkins–Johnson device. ——— Theoretical. ------ $n\lambda_g/2$ cavity modes. × Experimental. (b) Output power. ——— Short motion for increasing L. ------ Short motion for decreasing L. (c) Load resistance R_L. ——— Short motion for increasing L. ------ Short motion for decreasing L.

both Fig. 7(b) and (c), the solid curve corresponds to the short traveling away from the device; the dashed curve corresponds to motion of the short towards the device. The load resistance is seen to rise rapidly as the mode switching points are approached. In Fig. 7(b) the output power is plotted. It is seen that, in the mode switching region where the load resistance rises sharply, the power drops. Also the power falls as the short approaches 1.5 cm where the oscillations cease. Similar experimental observations of decreases in output power near mode switching points have been previously reported [4], [15]–[17]. The behavior shown in Fig. 7 is typical and is found for both full- and reduced-height waveguides.

VII. Summary and Conclusions

The theoretical equivalent circuits in which analytical expressions are used to describe all the elements adequately predicts and explains many properties of waveguide-mounted Gunn oscillators.

Certain aspects of the experimentally observed behavior of the oscillator are not predicted by the theoretical model discussed in this paper. However, it is reasonably certain that this is not due to any limitation of the proposed circuit model, but to the present lack of a device model capable of exhibiting the nonlinear dynamical behavior of the device. Therefore, some aspects of the interaction between the device and circuit are theoretically unpredictable.

Acknowledgment

The authors wish to thank R. Kiehl and A. Hern for assistance with experimental work; P. Blosser for computer programming; Prof. B. J. Leon, Prof. W. L. Weeks, and Prof. A. C. Kak for many helpful discussions; Dr. R. Eisenhart for making his thesis available to us; and Dr. W. K. Kennedy, Jr., of Watkins–Johnson for providing Gunn devices.

References

[1] E. Yamashita and J. R. Baird, "Theory of a tunnel diode oscillator in a microwave structure," *Proc. IEEE*, vol. 54, pp. 606–611, Apr. 1966.
[2] D. C. Hanson and J. E. Rowe, "Microwave circuit characteristics of bulk GaAs oscillators," *IEEE Trans. Electron Devices*, vol. ED-14, pp. 469–476, Sept. 1967.
[3] a) R. L. Eisenhart and P. J. Khan, "Theoretical and experimental analysis of a waveguide mounting structure," *IEEE Trans. Microwave Theory Tech.*, vol. MTT-19, pp. 707–719, Aug. 1971. b) R. L. Eisenhart, "Impedance characterization of a waveguide microwave circuit," Ph.D. dissertation, Univ. Michigan, Ann Arbor, 1970.
[4] W. C. Tsai, F. J. Rosenbaum, and L. A. MacKenzie, "Circuit analysis of waveguide cavity Gunn-effect oscillator," *IEEE Trans. Microwave Theory Tech. (Special Issue on Microwave Circuit Aspects of Avalanche-Diode and Transferred Electron Devices)*, vol. MTT-18, pp. 808–817, Nov. 1970.
[5] J. A. Bradshaw, "Scattering from a round metal post and gap," to be published.
[6] C. P. Jethwa and R. L. Gunshor, "Circuit characterization of waveguide-mounted Gunn-effect oscillators," *Electron. Lett.*, vol. 7, pp. 433–436, July 1971.
[7] K. Wilson, "Gunn effect devices and their applications," *Mullard Tech. Commun.*, vol. 10, pp. 286–293, July 1969.
[8] W. K. Kennedy, Jr., private communication.
[9] N. Marcuvitz, *Waveguide Handbook*, M.I.T. Rad. Lab. Ser., vol. 10. New York: McGraw-Hill, 1951, pp. 257–263.
[10] H. Jasik, *Antenna Engineering Handbook*. New York: McGraw-Hill, 1961, p. 7.
[11] L. Lewin, "A contribution to the theory of probes in waveguides," *Proc. Inst. Elec. Eng.*, monogr. 259R, pp. 109–116, July 1957.
[12] W. A. Edson, *Vacuum Tube Oscillators*. New York: Wiley, 1953, pp. 430–450.
[13] K. Kurokawa, "Some basic characteristics of broad band negative resistance oscillator circuits," *Bell. Syst. Tech. J.*, pp. 1937–1955, July–Aug. 1969.
[14] K. Kurokawa, J. P. Baccone, and N. D. Kenyon, "Broad band negative resistance oscillator circuits," *Int. Microwave Symp. Dig.*, pp. 281–284, 1969.
[15] B. C. Taylor, S. J. Fray, and S. E. Gibbs, "Frequency-saturation effects in transferred electron oscillators," *IEEE Trans. Microwave Theory Tech. (Special Issue on Microwave Circuit Aspects of Avalanche-Diode and Transferred Electron Devices)*, vol. MTT-18, pp. 799–807, Nov. 1970.
[16] H. J. Fossum, "Experimental investigation of x-band Gunn oscillators," Norwegian Defense Res. Establishment, Tech. Rep. TR-69-238, Jan. 1969.
[17] M. J. Howes, "Circuit considerations on the design of wide-band tunable transferred-electron oscillators," *IEEE Trans. Electron Devices*, vol. ED-17, pp. 1060–1067, Dec. 1970.
[18] R. J. Eisenhart and P. J. Khan, "Some tuning characteristics of waveguide-mounted Gunn-diode oscillators," presented at the IEEE Microwave Theory Tech. Int. Symp., May 1971.
[19] J. A. Copeland, "Theoretical study of a Gunn diode in a resonant circuit," *IEEE Trans. Electron Devices*, vol. ED-14, pp. 55–58, Feb. 1967.